Journal of Physics D: Applied Physics

PAPER

Ferromagnetic-resonance-induced spin pumping in $Co_{20}Fe_{60}B_{20}$/Pt systems: damping investigation

To cite this article: M Belmeguenai *et al* 2018 *J. Phys. D: Appl. Phys.* **51** 045002

IOP Publishing Journal of Physics D: Applied Physics
J. Phys. D: Appl. Phys. **51** (2018) 045002 (8pp) https://doi.org/10.1088/1361-6463/aa9f55

Ferromagnetic-resonance-induced spin pumping in $Co_{20}Fe_{60}B_{20}$/Pt systems: damping investigation

M Belmeguenai[1], M S Gabor[2], F Zighem[1], N Challab[1], T Petrisor Jr[2], R B Mos[2] and C Tiusan[2]

[1] LSPM (CNRS-UPR 3407), 99 avenue Jean-Baptiste Clément Université Paris 13, 93430 Villetaneuse, France
[2] Center for Superconductivity, Spintronics and Surface Science, Technical University of Cluj-Napoca, Str. Memorandumului No. 28, RO-400114, Cluj-Napoca, Romania

E-mail: belmeguenai.mohamed@univ-paris13.fr

Received 27 June 2017, revised 29 November 2017
Accepted for publication 5 December 2017
Published 8 January 2018

Abstract

Microstrip line ferromagnetic resonance (MS-FMR) has been used to investigate the dependence of the magnetic damping enhancement on the thickness of $Co_{20}Fe_{60}B_{20}$ and Pt due to spin pumping. Samples with variable thicknesses of $Co_{20}Fe_{60}B_{20}$ (Pt) are used to determine the spin mixing conductance (spin diffusion length) via the thickness dependence of the Gilbert damping parameter α of $Co_{20}Fe_{60}B_{20}$/Pt heterostructures. The results obtained from the analysis of the MS-FMR measurements reveal that α increases linearly with the inverse thickness of $Co_{20}Fe_{60}B_{20}$ for films capped with a 10 nm thick Pt layer, while the variation of α versus the Pt thickness of the 4 nm thick $Co_{20}Fe_{60}B_{20}$ layer has an exponential behaviour. The experimental data was analysed using a ballistic or a diffusive spin transport model for spin pumping, which includes the effective spin mixing conductance of the CoFeB/Pt interface and the spin-diffusion length of Pt. The estimated values are 37.5 nm^{-2} (spin mixing conductance) and 1.7 nm when the ballistic transport model is used, and 56.75 nm^{-2} and 2.2 nm when the experimental data are analysed using a more realistic model based on a diffusive transport. Moreover, MS-FMR measurements reveal that the effective magnetization varies linearly with the $Co_{20}Fe_{60}B_{20}$ inverse thickness due to the perpendicular interface anisotropy. This anisotropy, estimated to be 1.31 erg cm^{-2}, reinforces the perpendicular magnetization easy axis.

Keywords: magnetization dynamics, magnetic anisotropy, ferromagnetic resonance (FMR), Gilbert damping, spin pumping

(Some figures may appear in colour only in the online journal)

1. Introduction

The generation and manipulation of a spin current in nonmagnetic materials (NMs) is one of the pillars of modern spintronics [1]. Conventionally, spin currents are produced by passing a charge current through a thin ferromagnetic layer, whose magnetization direction can be controlled by an external magnetic field. Recently, several other routes, such as using the spin Hall effect (SHE) [1–4], the spin Seebeck effect [5, 6] or spin pumping [7, 8], have been used to generate spin currents.

Ferromagnetic resonance (FMR)-induced spin pumping is an emerging process for dynamically injecting a pure spin current into an NM without the need for a charge flowing, in contrast to SHE, for example. This involves a significant potential impact on the energy cost and on the efficiency of the spintronic devices. The resonant precession of ferromagnet (FM) magnetization pumps a spin current into the NM, which decays on a length scale called the spin-diffusion length (λ_{SD}). The value of this latter quantity is of great interest, since it would allow the efficiency of spin current

injection to increase in the FM/NM bilayer through optimization of the NM thickness [9]. Indeed, for a large NM thickness with respect to λ_{SD}, most of the spin current generated in the NM decays before returning to the FM interface due to the spin-flip scattering. On the other hand, with a small NM thickness (compared to λ_{SD}), the net spin current is reduced due to the spin diffusion caused by spin accumulating close to the NM surface. Furthermore, the spin injection process in the NM is accompanied by angular momentum loss in the FM leading to a broadening of the FMR linewidth, which is directly linked to the Gilbert damping parameter (α) [10]. This effect is more pronounced when the NM is a heavy metal with high spin–orbit coupling (SOC), due to the increased rate of spin scattering events, owing to the SOC. This opens the interesting possibility of tuning the damping value depending on the desired technological application. Another important quantity that characterizes the ability of the spin current to pass through the FM–NM interface, and thus the spin pumping efficiency, is the effective spin mixing conductance ($g_{\text{eff}}^{\uparrow\downarrow}$) [11].

Two models are usually used to describe this spin pumping effect on damping, and thus allow the determination of the spin diffusion length and the spin mixing conductance. These models are based on the evaluation of the net spin current (I^s) through the interface FM/NM ($I^s = I^{\text{pump}} - I^{\text{back}}$, where I^{pump} and I^{back} are the spin-pumped and the backflow spin currents, respectively). In the ballistic limit [12], λ_{SD} is much lower than the mean free path of electrons. Therefore, the NM is considered to be a perfect conductor and thus the I^{back} varies exponentially with the NM thickness [12]. In the diffusive model [13], the spin accumulation, generated by injected spins, is taken into account when calculating I^{back}. In this case, the damping enhancement is given by the effective spin mixing conductance, which depends *inter alia* on the finite electrical conductance of the NM.

In this paper, we determine the spin mixing conductance and the spin diffusion length in $Co_{20}Fe_{60}B_{20}$/Pt heterostructures from the investigation of the evolution of the Gilbert damping parameter versus the thicknesses of the $Co_{20}Fe_{60}B_{20}$ and the Pt layers. For this, we combined the microstrip line ferromagnetic resonance (MS-FMR) technique, where samples have been submitted in-plane or perpendicular to the plane magnetic applied fields and the vibrating sample magnetometry. Our investigation is based on an experimental procedure that minimizes the number of magnetic parameters involved in the fit of the experimental data (using the models presented below) as well as the extrinsic mechanism leading to FMR linewidth broadening. The obtained results demonstrate that the damping parameter varies linearly (exponentially) versus the $Co_{20}Fe_{60}B_{20}$ reciprocal thickness (versus the Pt thickness) due to spin pumping. Moreover, the effective magnetization deduced from the field dependence of the resonance frequency varies linearly with the $Co_{20}Fe_{60}B_{20}$ inverse thickness, suggesting the presence of perpendicular surface magnetic anisotropy.

2. Sample preparation and experimental methods

$Co_{20}Fe_{60}B_{20}$/Pt bilayers were grown at room temperature on thermally oxidized Si substrates. Two sets of samples were sputtered at room temperature and at a deposition pressure of 1 mtorr from two circular targets with a substrate target distance of 15 cm and a power of 5 W cm^{-2}: (i) $Co_{20}Fe_{60}B_{20}$ films with variable thicknesses ($t_{CFB} = 10$, 8, 6, 4 and 3 nm) capped by a 10 nm thick Pt layer and (ii) a 4 nm thick $Co_{20}Fe_{60}B_{20}$ film capped by a Pt layer of various thicknesses ($t_{Pt} = 1$, 2, 3, 4, 6, 8, 10 and 12 nm). The first (second) set of samples serves to determine the spin mixing conductance (spin diffusion length) from the investigation of the Gilbert damping parameter of the FM/NM heterostructures versus t_{CFB} (versus t_{Pt}). All samples were deposited on Si substrates covered with a 100 nm thick thermally oxidized SiO_2 layer by a magnetron sputtering system. For comparison, the 4.4 nm thick CoFeB layer capped with an 8 nm thick aluminium layer was grown on Si/SiO_2 in similar conditions. The static magnetic characteristics were investigated by using a vibrating sample magnetometer (VSM). For the dynamic measurements, we used the MS-FMR [14] technique, where the sample is mounted on a 0.5 mm wide microstrip line connected to a broadband microwave generator (operating in the range 0.1–20 GHz and applying a microwave power of 10 dBm) and a Schottky detector (operating in the frequency range of 2–18 GHz). Therefore, the frequency range measurement (2–18 GHz) is determined by the Schottky detector. The latter is connected to a lock-in amplifier to improve the signal-to-noise ratio. Therefore, the external magnetic field is modulated at 170 Hz by a small (4 Oe) alternating magnetic field and the measured signal is proportional to the field first derivative of the absorbed power. For each driven frequency, the sample is swept through the resonance by varying the applied static external field up to 1.9 T under an exciting microwave field with a power of 10 dBm. During the measurement, an external magnetic field H was applied perpendicular to the sample plane (for gyromagnetic ratio determination) or in-plane at various directions with respect to the sample edges (for all the other experimental data to be presented here) as indicated below. All the measurements presented here were taken at room temperature.

3. Results and discussions

The samples were characterized by x-ray diffraction via measurements of the 2θ-ω patterns (not presented here), which besides the substrate reflection, only show the presence of Pt (1 1 1) reflection. Due to the absence of any diffraction peaks corresponding to CoFeB, we conclude that these films have an isotropic in-plane crystallite distribution.

The principal aim of this work is the characterization of spin pumping in CoFeB/Pt thin films via the investigation of the thickness dependences of the damping. As will be shown below, for the precise determination of damping, spin mixing

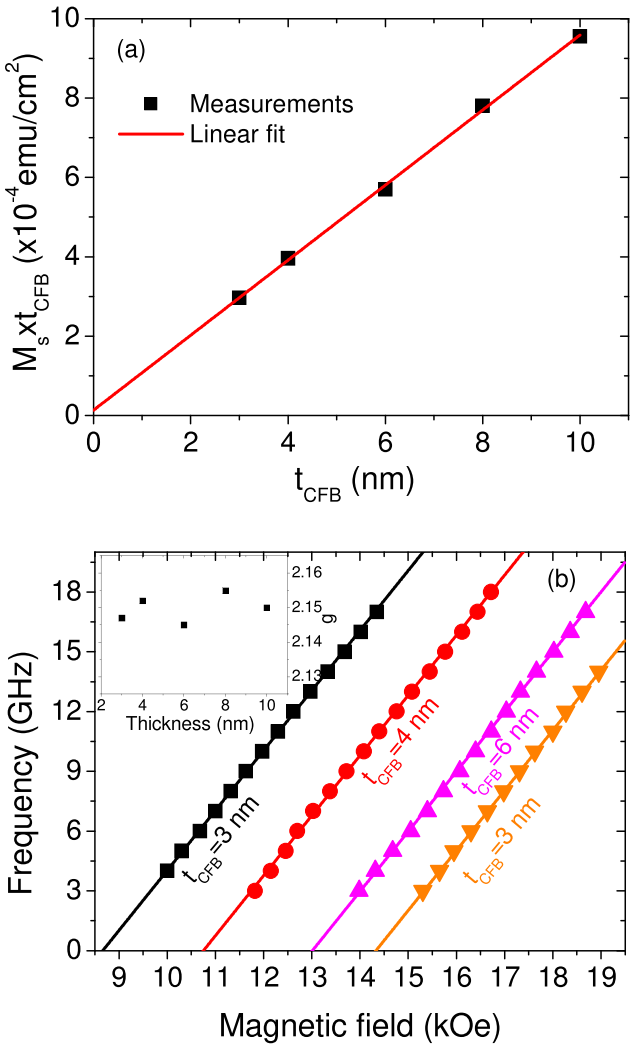

Figure 1. (a) Thickness dependence of the saturation magnetic moment per unit area for CoFeB films of various thicknesses (t_{CFB}) capped by a 10 nm thick Pt layer. (b) Variation of the uniform precession mode frequency as a function of the perpendicular applied magnetic field for $Co_{20}Fe_{60}B_{20}(t_{CFB})$/Pt(10 nm) heterostructures. The symbols refer to the experimental data and the solid lines are fits using equation (1). The inset of (b) shows the CoFeB thickness dependence of the g factor.

conductance and other magnetic parameters, the magnetization at saturation and the gyromagnetic ratio first need to be precisely evaluated. For this, the thickness dependences of the saturation magnetic moment per unit area were measured by VSM (as shown in figure 1(a) for CoFeB films capped by a 10 nm thick Pt layer) and then used to determine the magnetization at saturation and the magnetic dead layer: the slope gives the magnetization at saturation (M_s), while the horizontal axis intercept gives the extent of the magnetic dead layer. As indicated by figure 1(a), the magnetic dead layer thickness is nearly zero for this system, and the magnetization at saturation is around 945 ± 50 emu cm^{-3}. The obtained value of M_s is lower than that ($M_s \approx 1200$ emu cm^{-3}) of W/CoFeB/MgO [15] and Ta/CoFeB/Ta [16], but comparable to the one ($M_s = 800$–1100 emu cm^{-3}) obtained by Jang *et al* [17], Wang *et al* [18] and in [19]. The precise reason for this difference is not clearly understood at the moment. However, since the magnetization of thin film strongly depends on its interfaces and the crystallization degrees of CoFeB, we conclude that it is due to the lesser quality of our samples.

The g value, which determines the gyromagnetic factor γ, and which is involved in the precise determination of Gilbert damping and the effective magnetization, is precisely accessible by the MS-FMR technique, through the study of the frequency variation versus the amplitude of the magnetic field applied perpendicular to the film plane. The MS-FMR spectra (not shown here) display a single line, identified with the uniform precession mode. The resonance field of this mode is then obtained from the recorded spectra. The typical variations of the resonance frequency versus the perpendicular applied magnetic field are shown in figure 1(b) for various CoFeB thicknesses. Owing to the theoretical variations of the resonance frequency versus the magnetic field applied perpendicular to the film plane, given by equation (1), the best fits of the experimental data lead to the termination of $\gamma/2\pi$ and thus the Landé factor of the $Co_{20}Fe_{60}B_{20}$. As shown in the inset of figure 2(b), the obtained values of g are found to be mostly independent of the CoFeB thickness, and a unique value of $\gamma/2\pi = 30.13$ ($g = 2.15$) will be used for all the CoFeB thicknesses used in this study. This value is in good agreement with that obtained by Devolder [20] and Lee [21]

$$F_{\perp} = \mu_0 \left(\frac{\gamma}{2\pi}\right)(H - M_{\text{eff}}). \qquad (1)$$

$F_{\perp}$ is the uniform precession frequency corresponding to the magnetic field applied perpendicularly to the plane, $\mu_0 M_{\text{eff}} = \mu_0(M_s - H_{\perp})$ [14] refers to the effective magnetization and $H_{\perp}$ is the perpendicular magnetic anisotropy field. In the above expression, the small in-plane anisotropy fields have been neglected (as shown below), since the applied magnetic fields overpass the 0.9 T in the investigated frequency range, as shown in figure 1(b).

The Gilbert damping parameter controls how fast the magnetization reverses, and therefore it is an important technological parameter. Information on damping, and therefore on the relaxation mechanisms, can be obtained by measuring the FMR linewidth in the small magnetization precession amplitude regime (linear regime). This linewidth is caused by two mechanisms: the intrinsic damping (Gilbert damping) of the magnetization and extrinsic contributions (such as two magnon scattering [22], mosaicity [23], etc). The intrinsic damping processes are the unavoidable ones and the extrinsic contributions are eventually controllable. The angular and frequency dependences of the FMR linewidth provide information about these magnetic damping mechanisms. Figure 2(a) shows the typical MS-FMR angular dependence of the peak-to-peak field linewidth (ΔH^{PP}) at 8 GHz driven frequency, obtained from the Lorentzian derivative shaped MS-FMR spectra measured under a magnetic field applied in-plane. The observed pronounced anisotropy of the linewidth cannot be due to the Gilbert damping contribution, which is expected to be isotropic, and must be due to additional extrinsic damping mechanisms. These extrinsic contributions to the linewidth broadening are thickness-dependent and could lead to inappropriate intrinsic damping parameters and

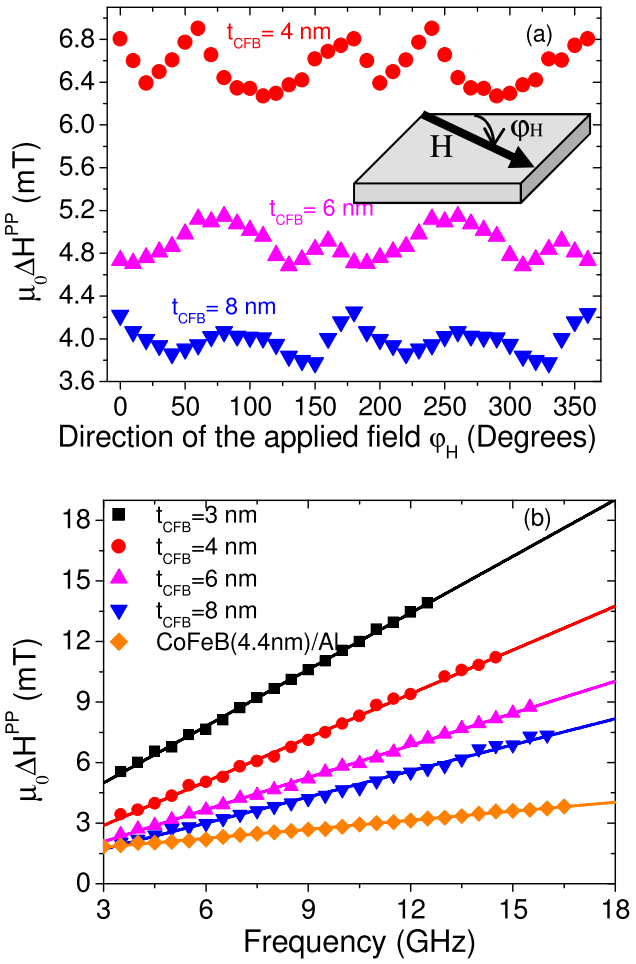

Figure 2. (a) The variation of the peak-to-peak FMR linewidth (ΔH^{PP}) versus the in-plane direction of the applied magnetic field with respect to the sample edge (φ_H) measured at 8 GHz driven frequency, and (b) peak-to-peak FMR field linewidth of the CoFeB thin films of a thickness t_{CFB} capped by the 10 nm Pt layer versus the driven frequency measured for a magnetic field applied in the direction where ΔH^{PP} is minimal ($\varphi_H = 0°$, 120°, 10° and 140° for $t_{CFB} = 3$, 4, 6 and 8 nm, respectively). For comparison, the measurements on CoFeB (4.4 nm)/Al (8 nm) are also presented for the applied field along the substrate edge ($\varphi_H = 0°$). The symbols refer to the experimental data and the solid lines are linear fits. The inset of figure (a) indicates a sketch for the direction of the applied field with respect to the sample edges.

spin mixing conductance. Due to the weak angular dependence of the linewidth (figure 2(a))—and since the main goal of this work is the investigation of the spin diffusion length and the spin mixing conductance—the identification of the extrinsic relaxation mechanisms and their variations as a function of the FM and of the NM thicknesses are not considered here. Therefore, the in-plane angular dependence of the resonance field for each sample is used to determine the applied field direction giving the minimum of ΔH^{PP}, and therefore the extrinsic contribution to the damping is minimal. This in-plane direction is found to be sample-dependent similar to the direction of the in-plane anisotropy easy axis (shown below), as shown in figure 2(a). The frequency dependence of ΔH^{PP} for the magnetic field applied along this in-plane direction giving the minimal ΔH^{PP} is illustrated in figure 2(b) for the CoFeB films capped by the 10 nm thick Pt layer. The observed linear behaviour confirms the main intrinsic contribution to damping. The ΔH^{PP} of CoFeB/Pt is significantly higher when compared to that corresponding to CoFeB(4.4 nm)/Al(8 nm), as can be seen from figure 2(b), suggesting a capping layer effect. To extract the Gilbert damping constant, we simply consider that ΔH^{PP} shows the following dependence on α [23, 24]:

$$\mu_0\Delta H^{PP} = \mu_0\Delta H_0^{PP} + \frac{2}{\sqrt{3}}\frac{\alpha}{\gamma}2\pi f \qquad (2)$$

where f is the driven frequency and ΔH_{00}^{PP} is the inhomogeneous residual linewidth, which is frequency independent. The multiplying factor of $\frac{1}{\sqrt{3}}$ in equation (2), is the correction factor of the difference between the full width at half maximum and the peak-to-peak linewidths for the line shape of the Lorentzian [24].

The obtained results from the fit of the experimental data (presented in figure 2(b)), using equation (2), are shown in figure 3(a). This reveals that the Gilbert damping constant increases linearly with $1/(t_{CFB})$ due to the spin pumping current induced in Pt by the FMR precession of the magnetization and thus a loss of the angular momentum. The amount of spin pumping is closely related to the SOC through the spin flip relaxation time and the $g_{eff}^{\uparrow\downarrow}$, which we aim to determine below. Moreover, it should be mentioned that the inhomogeneity contribution to the linewidth broadening ΔH_0^{PP} decreases as the CFB thickness increases.

By considering that the total damping is given by $\alpha = \alpha_{CFB} + \alpha_{pump}$ [25], where α_{CFB} is the Gilbert damping constant of the CoFeB and α_{pump} is the damping introduced by the spin pumping effect due to Pt, the linear fit of the experimental data of figure 3(a) (red line) gives $\alpha_{CFB} \approx 0.0034 \pm 0.0005$. This value is slightly lower than that of the bulk $Co_{40}Fe_{40}B_{20}$ ($\alpha_{CFB} = 0.004$) [26]. It is also slightly lower than the obtained value ($\alpha_{CFB} = 0.0039$) for CoFeB(4.4 nm)/Al(8 nm), where the spin pumping contribution from aluminium is expected to be very weak. The spin pumping contribution to the damping is given by $\alpha_{pump} = \frac{g\mu_B}{4\pi M_s t_{CFB}} g^{\uparrow\downarrow}$ [8, 27], where μ_B is the Bohr magneton, g is the Landé factor and $g^{\uparrow\downarrow}$ is the intrinsic spin mixing conductance of the interface CoFeB/Pt. This expression is only valid for thick enough NM layers with respect to λ_{SD}, where no reflection of the spin current takes place at the interfaces. The experimental data shown in figure 3(a) has been analysed using this model for spin pumping, leading to $g^{\uparrow\downarrow} = 37.5 \pm 3\,nm^{-2}$, which is higher than that of YIG/Pt (18 nm^{-2}) [28] and lower than that of the $Co_{32}Fe_{48}B_{20}$/Pt (50.7 nm^{-2}) [29] systems. This value is also lower than that of $Co_{40}Fe_{40}B_{20}$/Pt obtained by Ruiz-Calaforra *et al* (40 nm^{-2}) [30] and by Conca *et al* (61 nm^{-2}) [31]. In the latter case, the authors attributed their higher value to the contribution of the proximity magnetization effect induced in Pt. By subtracting this contribution, a lower value of 49 nm^{-2} was obtained. The lower measured magnetization at the saturation of our samples compared to the obtained ones in [30, 31] suggests the lesser quality of our samples and may be the reason for this smaller spin mixing conductance.

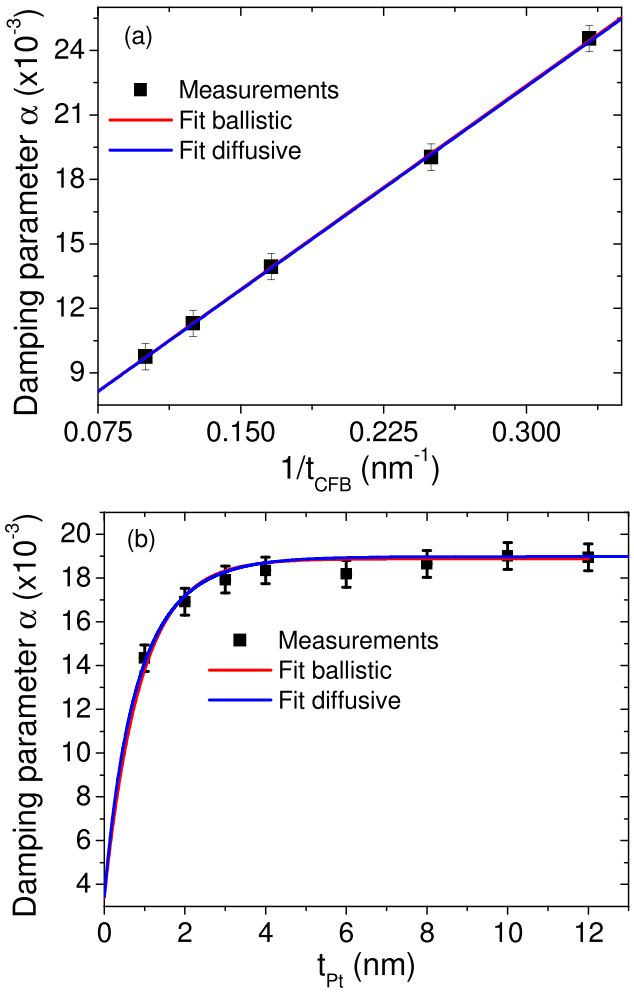

Figure 3. (a) The CoFeB thickness dependence of the Gilbert damping parameter of CoFeB thin films of a thickness t_{CFB} capped by a 10 nm thick Pt layer, deduced from figure 2(b) using equation (2). The symbols refer to the experimental data and the solid lines are fits using models based on the ballistic (red line) and the diffusive (blue line) spin transport described in the paper. (b) The Gilbert damping constant versus the thickness (t_{Pt}) of the Pt capping layer of the 4 nm thick CoFeB thin films. The symbols refer to the experimental data and the solid lines are fits using equations (3) and (4) for the red and blue lines, respectively.

The spin diffusion length is a fundamental parameter in the study of spin-dependent transport. Various methods such as the lateral spin valve [32], SHE, spin pumping [33] and spin-torque FMR [34] have proven their efficiency when measuring λ_{SD}. To determine λ_{SD}, the dependence of α versus the Pt thickness was investigated for the 4 nm thick CoFeB layer, as shown in figure 3(b). One can observe an exponential behaviour, which is another sign of spin pumping in these samples. To determine λ_{SD}, two models were considered: ballistic and diffusive transports. Within ballistic transport, the dependence of damping on the HM capping layer thickness (Pt here) exhibits a simple exponential dependence of the Pt thickness as described by [12, 35]:

$$\alpha = \alpha_{CFB} + \frac{g\mu_B}{4\pi M_s t_{CFB}} g^{\uparrow\downarrow}\left[1 - e^{\frac{-2t_{Pt}}{\lambda_{SD}}}\right]. \quad (3)$$

By fitting the experimental data of figure 3(b) (red line) with equation (3) and using the same values of α_{CFB} ($\alpha_{CFB} \approx 0.0034 \pm 0.0005$) and the spin mixing conductance ($g^{\uparrow\downarrow} = 37.5 \pm 3\,nm^{-2}$) obtained from the CoFeB thickness dependence of damping (figure 3(a)), we determine the λ_{SD} of Pt to be 1.7 nm. As we mentioned above, equation (3) is an approximation, since the thickness of the sample is assumed to be less than the mean free path, and the resistance of the MN materials is neglected. In order to determine the true intrinsic spin mixing conductance values, more rigorous treatment is needed. A quantitative analysis based upon diffusive transport, which could improve the accuracy of the fitted parameters, has been presented by Boone *et al* [36, 37]. In this analysis, the spin pumping contribution to damping depends strongly on both the spin and charge transport properties of the NM. It allows the accurate determination of the intrinsic spin mixing conductance, in contrast to the ballistic transport model. According to Boone *et al*, the additional damping due to spin pumping is given by:

$$\alpha_{pump} = \frac{g\mu_B}{4\pi M_s t_{CFB}} \frac{g^{\uparrow\downarrow}}{1 + \frac{g^{\uparrow\downarrow}}{g_{ext}}} \quad (4)$$

where $g^{\uparrow\downarrow}$ is the intrinsic spin mixing conductance of CoFeB/Pt (which determines how much spin current passes through the interface), σ_{Pt} is the electrical conductance of Pt and g_{ext} is given by $g_{ext} = \frac{h}{e^2}\frac{\sigma_{Pt}}{\lambda_{SD}} \tanh\left(\frac{t_{Pt}}{\lambda_{SD}}\right)$ [13], for a simple FM/NM interface. Note that $g_{eff}^{\uparrow\downarrow} = \frac{g^{\uparrow\downarrow}}{1+\frac{g^{\uparrow\downarrow}}{g_{ext}}}$ governs the spin pumped out of the ferromagnetic material in contrast to the ballistic model. This takes into account the finite electrical resistance of the NM material, which depends on the preparation conditions and on the sample quality. Therefore, this effective spin mixing conductance is not as useful, since it cannot really be applied to samples made in other conditions, and intrinsic spin mixing conductance should be given when characterizing the spin pumping efficiency.

By self-consistent fitting of both the thickness dependencies of damping shown in figure 3, using this model (blue line) and σ_{Pt} given in [36], we determine the intrinsic mixing conductance of CoFeB/Pt and the spin diffusion length of Pt, estimated to be $56.75 \pm 4\,nm^{-2}$ and 2.2 nm, respectively. Note here the enhancement of the accuracy for the determination of the intrinsic spin-mixing conductance CoFeB/Pt interface, as well as the spin diffusion length, since a self-consistent fitting of the data for samples with varying NM and FM layer thicknesses is used. We should mention the discrepancy of the published values of the spin diffusion length (due to the interface quality difference) for Pt, ranging from 1 to 10 nm [38]. Therefore, the obtained values here of λ_{SD} using the two models are within this range. Note that for the spin mixing conductance, the effective value should always be smaller than the intrinsic one since the backflow spin current has to be taken into account for $g_{eff}^{\uparrow\downarrow}$. Therefore, $g_{eff}^{\uparrow\downarrow}$ cannot be used as a good approximation for the intrinsic spin-mixing conductance, especially in our samples. It is worth mentioning that due to the lack of experimental proof that spin transport can proceed via ballistic channels in metallic multilayer structures

when thicknesses are less than the mean free path [36], the diffusive model remains more realistic for experimental data analysis.

We also investigate another important technological and interfacial effect by determining the perpendicular anisotropy field using the MS-FMR measurements under an in-plane applied magnetic field. For a more precise determination of this field, the in-plane anisotropy field should be taken into account when fitting the measurements. Therefore, the variation of the uniform precession mode resonance field versus the direction of the in-plane applied magnetic field is used to determine the in-plane anisotropy type and field. Then, the resonance frequency of this mode is measured versus the applied magnetic field along a given direction (usually the hard or easy axis direction) and fitted to determine the effective magnetization taking into account the typical value of the gyromagnetic ratio, previously determined. Figure 4(a) shows the angular dependence of the resonance field of different CoFeB thin films capped by a 10 nm thick Pt layer. It shows that the angular behaviour is governed by a small uniaxial anisotropy (not exceeding 5 mT). The anisotropy easy axis direction depends on the sample. This behaviour has been confirmed by measuring the hysteresis loops by VSM with an in-plane magnetic field applied along various orientations φ_H with respect to the sample edges. Figure 4(b) shows the typical in-plane (along the easy and the hard axes) magnetization loops for the 4 nm thick $Co_{20}Fe_{60}B_{20}$ (CFB) film capped by a 3 nm thick Pt layer. The easy axis magnetization hysteresis curve presents a square loop with a coercive field of about 1 mT. For the measurements along the hard axis, a slightly tilted loop with a significantly smaller remanence appears once the applied field is perpendicular to the easy axis direction. The uniaxial anisotropy is around 5 mT, as can be determined from the saturation field in the hard axis direction. Since the goals of this paper are the spin pumping and the perpendicular magnetic anisotropy, the in-plane anisotropy nature, its origin and their thickness dependences will not be considered here. The corresponding field dependence of the uniform precession mode frequency recorded for an applied field along the hard (for $t_{CFB} = 4$ nm) or along the easy axis (for other thicknesses) are shown in figure 4(c). To determine the perpendicular anisotropy field of the CFB films, the in-plane angular dependence of the resonance field and the evolution of the resonance frequency versus the magnetic in-plane applied field, shown in figure 4, have been analysed. The used model is based on the magnetic energy density characterized by Zeeman, demagnetizing, in-plane and perpendicular to the plane uniaxial anisotropy energies. Therefore, as discussed in [39], the resonance frequency for a magnetic field applied in-plane at an angle of φ_H with respect to the sample edges can be obtained from the energy density as [14]:

$$F_{//}^2 = \left(\mu_0 \tfrac{\gamma}{2\pi}\right)^2 [H\cos(\varphi_H - \varphi_M) + H_u \cos 2(\varphi_M - \varphi_u)] \times \left[H\cos(\varphi_H - \varphi_M) + M_{eff} + \tfrac{H_u}{2}(1 + \cos 2(\varphi_M - \varphi_u))\right] \quad (5)$$

where $F_{//}$ is the uniform precession frequency for the magnetic field applied in-plane, φ_M (φ_H) and φ_u are angles defining the

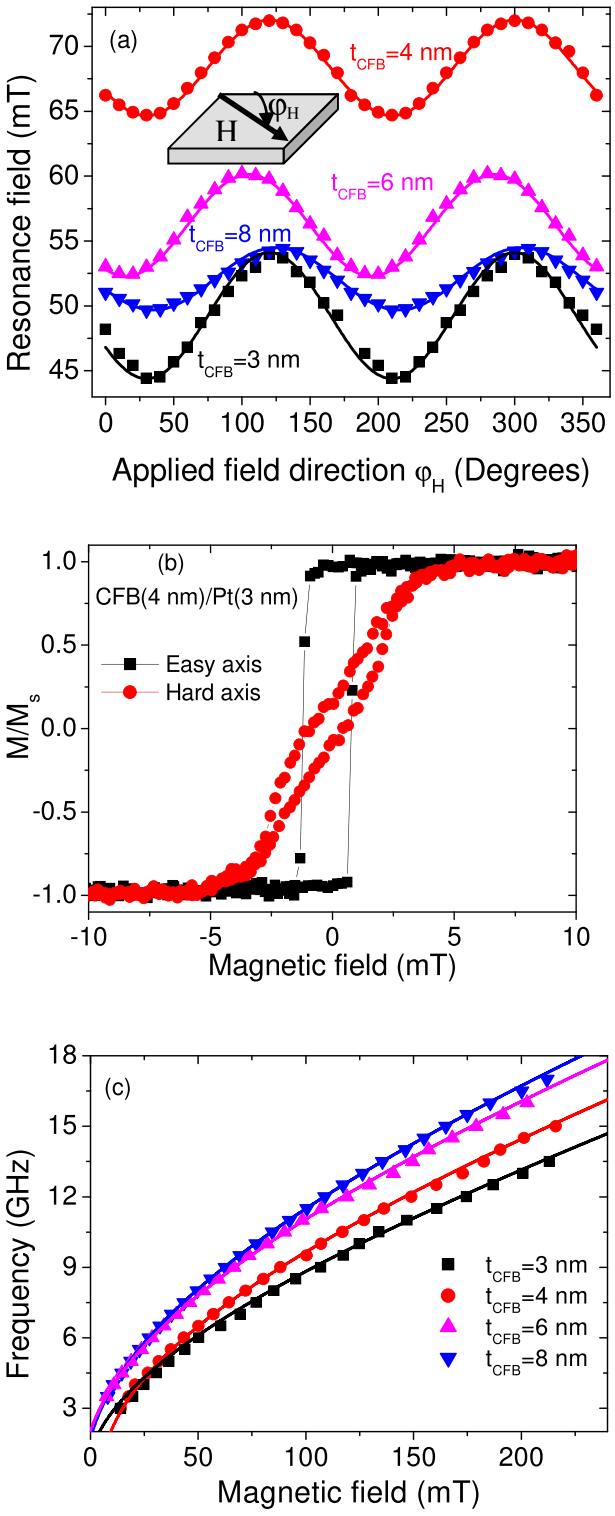

Figure 4. (a) The resonance field of CoFeB (t_{CFB})/Pt (10 nm) versus the direction of the in-plane applied field with respect to the sample edge (φ_H) measured at 6 GHz (for $t_{CFB} = 3$ nm) and 8 GHz (for other CFB thicknesses) driving frequencies. (b) The in-plane magnetization hysteresis curves for the CFB (4 nm)/Pt (3 nm). (c) The hard ($t_{CFB} = 4$ nm) and easy (other thicknesses) axes field dependences of the resonance frequency for CFB thin films of a thickness t_{CFB} capped with a 10 nm thick Pt layer. The symbols refer to the experimental data and the solid lines are fits using equation (5). The inset of figure (a) indicates a sketch for the direction of the applied field with respect to the sample edges.

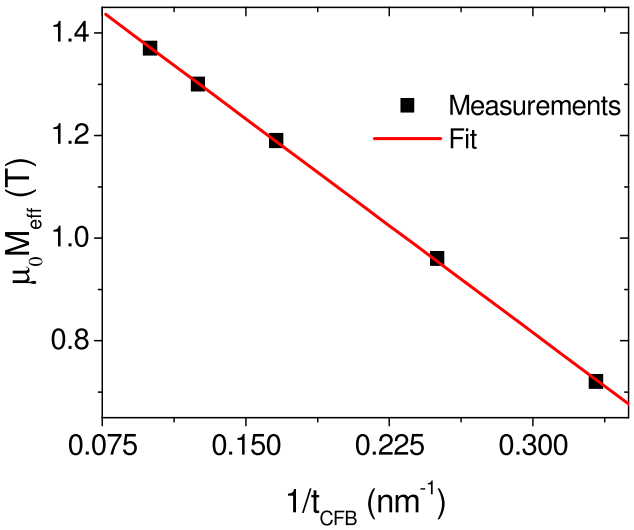

Figure 5. The thickness dependence of the effective magnetization ($M_{\rm eff}$) extracted from the fit of the FMR measurements for the CFB thin films of a thickness $t_{\rm CFB}$ capped with a 10 nm thick Pt layer. The symbols refer to the experimental data and the solid lines are linear fits.

directions of the magnetization (the applied field) and of the planar uniaxial anisotropy easy axis with respect to the substrate edges, respectively; $H_{\rm u}$ is the uniaxial in-plane anisotropy field.

As we mentioned above, the uniaxial anisotropy fields in our samples are very weak. Therefore, these fields are very low compared to the resonance fields at the driven frequencies used in this work (2–18 GHz). Indeed, in this condition, the magnetization direction will be almost parallel to the applied magnetic field ($\varphi_M = \varphi_H$). Consequently, equation (5) can be more simplified and the resonance field ($H_{\rm r}$) is thus given by equation (6).

$$H_{\rm r} = \frac{1}{2}\sqrt{\left(M_{\rm eff} + H_{\rm u}\sin^2(\varphi_H - \varphi_{\rm u})\right)^2 + 4\left(\frac{2\pi F_{//}}{\mu_0\gamma}\right)^2} - \frac{M_{\rm eff}}{2} - \frac{H_{\rm u}}{4}\left(1 + 3\cos 2(\varphi_H - \varphi_{\rm u})\right). \quad (6)$$

Equation (6) is obtained by solving the quadratic equation which is directly deduced from the simplified form of equation (5).

Figure 5 plots the extracted effective magnetization versus the inverse film thickness $1/t_{\rm CFB}$, where it can be seen that $M_{\rm eff}$ follows a linear variation. We conclude that the perpendicular anisotropy field includes a surface energy term. Therefore, the effective perpendicular anisotropy constant $K_\perp$ (with $\mu_0 H_\perp = 2K_\perp/M_{\rm s}$) can be phenomenologically separated into volume and interface contributions and approximately obeys the relation $K_\perp = K_{\rm v} + K_{\rm s}/t_{\rm CFB}$ [40, 41]. This allows us to derive the perpendicular surface and volume anisotropy constants $K_{\rm s} = 1.31$ erg cm^{-2} and $K_{\rm v} = -2.18 \times 10^6$ erg cm^{-3}, respectively. Being negative, the volume contribution provides an in-plane reinforcement of the anisotropy easy axis, while the positive surface one (most probably induced by Pt) favours a perpendicular magnetization easy axis. This surface anisotropy constant is larger than those of Pt/Co (0.5–0.58 erg cm^{-2}) [42] and Ta/Pt/Co/AlO$_x$ ($K_{\rm s} = 1.1$ erg cm^{-2}) [43]. We should mention that a high perpendicular anisotropy can induce inhomogeneous magnetization that can also increase damping. Such extrinsic contributions to damping should lead to nonlinear variation in the linewidth versus frequency. In contrast, when the damping is purely Gilbert damping, the FMR linewidth varies linearly with the frequency, and the damping parameter α is extracted from the slope of the line. From the theory of spin pumping, the additional damping term ($\Delta\alpha$) is Gilbert-type damping. Therefore, according to the theory [10], if the additional damping is caused by spin pumping, then the linewidth which contains $\alpha + \Delta\alpha$ should vary linearly versus the microwave frequency. As shown in figure 2(b), it is clearly seen for all the samples that $\Delta H^{\rm PP}$ varies linearly with frequency, leading to the conclusion that $\Delta\alpha$ is Gilbert-type and not caused by any other processes. Therefore, the used measurement scheme, which consists of determining the direction of the applied field giving the minimal value of $\Delta H^{\rm PP}$, seems to be efficient enough to avoid any extrinsic contributions to damping such as anisotropy-induced inhomogeneous magnetization.

4. Conclusion

CoFeB/Pt heterostructures with variable CoFeB and Pt thicknesses were grown by sputtering on thermally oxidized Si substrates. MS-FMR has been used to investigate the thickness dependences of the Gilbert damping constant, and therefore to measure both the spin diffusion length and the spin mixing conductance in CoFeB/Pt systems, using two models based on diffusive or ballistic spin transport. To minimize the number of the parameters to be used for the experimental data fit, the magnetization at saturation and the gyromagnetic ratio were measured. Moreover, to increase the accuracy of the determination of the intrinsic damping parameter, the in-plane angular dependence of the linewidth was systematically measured to obtain the applied field direction where the extrinsic contributions are minimal. The deduced Gilbert damping constant was found to vary linearly (exponentially) versus the CoFeB (Pt) thickness due to the spin pumping induced by the FMR. The obtained results demonstrate the efficiency of the possibility of tuning the Gilbert damping constant by a judicial choice of nonmagnetic layer, depending on the desired application. Finally, the thickness dependence of the perpendicular anisotropy field revealed an interfacial contribution estimated to be 1.31 erg cm^{-2}.

Acknowledgments

This work has been supported by the Conseil regional d'Île-de-France through the DIM NanoK (BIDUL project). MSG and TP acknowledge the financial support of UEFISCDI through PN-II-RU-TE-2014-1820—SPINCOD research grant No. 255/01.10.2015.

ORCID iDs

M Belmeguenai https://orcid.org/0000-0002-2395-1146
M S Gabor https://orcid.org/0000-0003-0888-0762
F Zighem https://orcid.org/0000-0003-3392-8238

References

[1] Sinova J, Valenzuela S O, Wunderlich J, Back C H and Jungwirth T 2015 *Rev. Mod. Phys.* **87** 1213
[2] Wunderlich J, Kaestner B, Sinova J and Jungwirth T 2005 *Phys. Rev. Lett.* **94** 047204
[3] Hirsch J E 1999 *Phys. Rev. Lett.* **83** 1834
[4] Kato Y K, Myers R C, Gossard A C and Awschalom D D 2004 *Science* **306** 1910
[5] Adachi H, Uchida K, Saitoh E and Maekawa S 2013 *Rep. Prog. Phys.* **76** 036501
[6] Uchida K, Takahashi S, Harii K, Ieda J, Koshibae W, Ando K, Maekawa S and Saitoh E 2008 *Nature* **455** 778
[7] Brataas A, Tserkovnyak Y, Bauer G E W and Halperin B I 2002 *Phys. Rev.* B **66** 060404
[8] Tserkovnyak Y, Brataas A, Bauer G E W and Halperin B I 2005 *Rev. Mod. Phys.* **77** 1375
[9] Ulrichs H, Demidov V E, Demokritov S O, Lim W L, Melander J, Ebrahim-Zadeh N and Urazhdin S 2013 *Appl. Phys. Lett.* **102** 132402
[10] Tserkovnyak Y, Brataas A and Bauer G E W 2002 *Phys. Rev. Lett.* **88** 117601
[11] Chudo H, Ando K, Saito K, Okayasu S, Haruki R, Sakuraba Y, Yasuoka H, Takanashi K and Saitoh E 2011 *J. Appl. Phys.* **109** 073915
[12] Foros J, Woltersdorf G, Heinrich B and Brataas A 2005 *J Appl. Phys.* **97** 10A714
[13] Tserkovnyak Y, Brataas A and Bauer G E W 2002 *Phys. Rev.* B **66** 224403
[14] Belmeguenai M, Zighem F, Roussigné Y, Chérif S M, Moch P, Westerholt K, Woltersdorf G and Bayreuther G 2009 *Phys. Rev.* B **79** 024419
[15] Pai C-F, Nguyen M-H, Belvin C, Vilela-Leão L H, Ralph D C and Buhrman R A 2014 *Appl. Phys. Lett.* **104** 082407
[16] Jhajhria D, Pandya D K and Chaudhary S 2016 *RSC Adv.* **6** 94717
[17] Jang S Y, You C-Y, Lim S H and Lee S R 2011 *J. Appl. Phys.* **109** 013901
[18] Wang Y-H, Chen W-C, Yang S-Y, Shen K-H, Park C, Kao M-J and Tsai M-J 2006 *J. Appl. Phys.* **99** 08M307
[19] Wang K, Xu Z, Huang Y, Qiu Y and Dong S 2016 *Sci. China Mater.* **59** 639
[20] Devolder P-H, Ducrot T, Adam J-P, Barisic I, Vernier N, Kim J-V, Ockert B and Ravelosona D 2013 *Appl. Phys. Lett.* **102** 022407
[21] Lee H, Wen L, Pathak M, Janssen P, LeClair P, Alexander C, Mewes C K A and Mewes T 2008 *J. Phys. D: Appl. Phys.* **41** 215001
[22] Srivastava A K, Hurben M J, Wittenauer M A, Kabos P, Patton C E, Ramesh R, Dorsey P C and Chrisey D B 1999 *J. Appl. Phys.* **85** 7838
[23] Zakeri Kh *et al* 2007 *Phys. Rev.* B **76** 104416
[24] Mizukami Y, Ando S and Miyazaki T 2002 *Phys. Rev.* B **66** 104413
[25] Nakayama H, Ando K, Harii K, Yoshino T, Takahashi R, Kajiwara Y, Uchida K, Fujikawa Y and Saitoh E 2012 *Phys. Rev.* B **85** 144408
[26] Liu X, Zhang W, Carter M J and Xiao G 2011 *J. Appl. Phys.* **110** 033910
[27] Jiao H J and Bauer G E W 2013 *Phys. Rev. Lett.* **110** 217602
[28] Qiu Z, Ando K, Uchida K, Kajiwara Y, Takahashi R, Nakayama T, An H, Fujikawa Y and Saitoh E 2013 *Appl. Phys. Lett.* **103** 092404
[29] Kim D-J, Il Kim S, Park S-Y, Lee K-D and Park B-G 2014 *Curr. Appl. Phys.* **14** 1344
[30] Ruiz-Calaforra A, Brächer T, Lauer V, Pirro P, Heinz B, Geilen M, Chumak A V, Conca A, Leven B and Hillebrands B 2015 *J. Appl. Phys.* **117** 163901
[31] Conca A, Heinz B, Schweizer M R, Keller S, Papaioannou E Th and Hillebrands B 2017 *Phys. Rev.* B **95** 174426
[32] Laczkowski P, Vila L, Nguyen V-D, Marty A, Attané J-P, Jaffrès H, George J-M and Fert A 2012 *Phys. Rev.* B **85** 220404
[33] Zhang W, Vlaminck V, Pearson J E, Divan R, Bader S D and Hoffmann A 2013 *Appl. Phys. Lett.* **103** 242414
[34] Liu L, Moriyama T, Ralph D C and Buhrman R A 2011 *Phys. Rev. Lett.* **106** 036601
[35] Shaw J M, Nembach H T and Silva T J 2012 *Phys. Rev.* B **85** 054412
[36] Boone C T, Nembach H T, Shaw J M and Silva T J 2013 *J. Appl. Phys.* **113** 153906
[37] Boone C T, Shaw J M, Nembach H T and Silva T J 2015 *J. Appl. Phys.* **117** 223910
[38] Rojas-Sánchez J-C, Reyren N, Laczkowski P, Savero W, Attané J-P, Deranlot C, Jamet M, George J-M, Vila L and Jaffrès H 2014 *Phys. Rev. Lett.* **112** 106602
[39] Farle M 1998 *Rep. Prog. Phys.* **61** 755
[40] Johnson M T, Bloemen P J H, den Broeder F J A and de Vries J J 1996 *Rep. Prog. Phys.* **59** 1409
[41] Kaidatzis A, Bran C, Psycharis V, Vázquez M, García-Martín J M and Niarchos D 2015 *Appl. Phys. Lett.* **106** 262401
[42] den Broeder F J A, Hoving W and Bloemen P J H 1991 *J. Magn. Magn. Mater.* **93** 562
[43] Kim N-H, Han D-S, Jung J, Cho J, Kim J-S, Swagten H J M and You C-Y 2015 *Appl. Phys. Lett.* **107** 142408